HHS Public Access

Author manuscript

Invest Radiol. Author manuscript; available in PMC 2024 January 01.

Published in final edited form as:

Invest Radiol. 2023 January 01; 58(1): 99–110. doi:10.1097/RLI.0000000000000908.

Computed Tomography: State-of-the-Art Advancements in Musculoskeletal Imaging

Hamza Ahmed Ibad, M.B.B.S[1], **Cesar de Cesar Netto, MD, PhD**[2], **Delaram Shakoor, MD**[3], **Alejandro Sisniega, PhD**[4], **Stephen Liu, BS**[4], **Jeffrey H Siewerdsen, PhD**[4], **John A. Carrino, MD, MPH**[5], **Wojciech Zbijewski, PhD, MS**[4], **Shadpour Demehri, MD**[1]

[1.]The Russell H. Morgan Department of Radiology and Radiological Science, Johns Hopkins University School of Medicine, Baltimore, MD, USA

[2.]Department of Orthopaedics and Rehabilitation, Carver College of Medicine, University of Iowa, Iowa City, IA, USA

[3.]Department of Radiology and Biomedical Imaging, Yale School of Medicine, New Haven, CT, USA

[4.]Department of Biomedical Engineering, Johns Hopkins University, Baltimore, MD, USA.

[5.]Department of Radiology and Imaging, Hospital for Special Surgery, New York, NY, USA.

Abstract

While musculoskeletal magnetic resonance imaging (MRI) plays a dominant role in characterizing abnormalities, novel CT techniques have found an emerging niche in several scenarios such as trauma, gout, and the characterization of pathologic biomechanical states during motion and weight-bearing. Recent developments and advancements in the field of musculoskeletal computed tomography include four-dimensional (4D), cone-beam (CB), and dual-energy (DE) computed tomography (CT). Four-dimensional (4D) CT has the potential to quantify biomechanical derangements of peripheral joints in different joint positions to diagnose and characterize patellofemoral instability, scapholunate ligamentous injuries, and syndesmotic injuries. CBCT provides an opportunity to image peripheral joints during weight-bearing, augmenting the diagnosis and characterization of disease processes. Emerging CBCT technologies improved spatial resolution for osseous microstructures in the quantitative analysis of osteoarthritis-related subchondral bone changes, trauma, and fracture healing. DECT-based material decomposition visualizes and quantifies monosodium urate crystals in gout, bone marrow edema in traumatic and nontraumatic fractures, and neoplastic disease. Recently, DE techniques have been applied to CBCT, contributing to increased image quality in contrast-enhanced arthrography, bone densitometry, and bone marrow imaging. This review describes 4DCT, CBCT, and DECT advances, current logistical limitations, and prospects for each technique.

Corresponding Author: Wojciech Zbijewski, PhD, MS. Johns Hopkins University, Traylor Building, 720 Rutland Avenue, Baltimore, MD, 212052109, Phone: 410-955-1319, wzbijewski@jhu.edu.

Conflicts of Interest and Source of Funding:
All authors declare no conflicts of interests.

Keywords

Computed Tomography; Four-dimensional CT; Dynamic CT; Cone-beam CT; Dual-energy CT; patellofemoral instability; gout; trauma; fracture; healing

Introduction

Recent advances in computed tomography (CT) have enabled the volumetric acquisition of images of the musculoskeletal system, preceding similar capability in magnetic resonance imaging (MRI)[1–4]. The acquired small (0.3–0.5 mm) isotropic voxels can be reconstructed into conventional (axial, coronal, and sagittal) and nonconventional planes using multiplanar reformation (MPR), resulting in detailed characterizations of the bone and soft tissue components of the musculoskeletal system.

In musculoskeletal disease and peripheral joint injury, there is an overwhelming preference for MRI use due to its superior inherent contrast resolution making it highly reliable in identifying subtle soft-tissue injuries involving tendons, ligaments, muscles, and articular cartilage[5,6]. However, emerging advances in CT technology have provided exciting opportunities to examine the musculoskeletal system in situations more suited to faster examinations - in time-sensitive and emergent clinical settings such as acute trauma. In addition, these innovations also allow CT to be used in circumstances where MRI is clinically contraindicated or unfeasible. (e.g., in-situ pacemaker and claustrophobia)[7].

Since the development of the first-generation CT in 1967, each successive generation has reduced data acquisition times with the progressive introduction of multiple detectors and narrow X-ray beams (2nd generation CT); rotate geometry and wide X-ray beams (3rd generation CT); and rotating X-ray tubes and stationary ring detectors (4th generation CT), with the advent of slip-ring technology further drastically decreasing acquisition times. Novel multidetector CT (MDCT), with multiple rows of detectors, allows volume data acquisition instead of per slice data[8] and is the current technique of choice for musculoskeletal studies.

Several emerging CT acquisition techniques have been developed and validated specifically for musculoskeletal applications, including four-dimensional CT (4DCT) allowing examination of peripheral joints in motion, cone-beam CT (CBCT) enabling weight-bearing examinations, and dual-energy CT (DECT) enabling spectral and material-specific imaging. When appropriately used in clinical practice, these techniques can greatly impact and add diagnostic value complementing MRI in patients with various musculoskeletal disorders.

In this review article, we discuss the role and unique diagnostic values of 4DCT, CBCT, and DECT in musculoskeletal imaging to detect and characterize various musculoskeletal abnormalities and peripheral joint injuries.

Four-Dimensional Computed Tomography

Four-dimensional computed tomography (4DCT) is a CT technique employed to perform imaging acquisition of a specific anatomical area of interest over a fourth dimension: time.

4DCT of peripheral joints is commonly acquired through sequential yet non-continous scans of a joint during predefined motions (e.g., flexion-extension of the tibiofemoral joint) at different joint positions. Using predefined and validated protocols, examinees are trained by the CT technologists to complete specific motions within certain time frames to optimize the detection of dynamic biomechanical derangements. At each discrete time point, the obtained volumetric CT acquisition is integrated and combined to create multiple consecutive 3D volumes over time.

Due to the sheer volume of data required to complete such a study, specific care must be taken to optimize spatial and temporal resolution while reducing scanning times and radiation exposure. The principles remain the same as in a conventional study. Scan times are improved through increased gantry speed, which is inversely related to the number of projections acquired, consequently having a negative impact on image quality[9]. However, image quality can be improved while maintaining low scan times by employing several techniques such as iterative reconstruction, which uses data from adjacent time-frames to reconstruct a particular volume[10].

Radiation Exposure

Effective radiation doses for 4DCT examinations are higher than their single-acquisition MDCT equivalents. For example, the average 4DCT examination of the knee has an effective dose of 1.57 mSv (single-acquisition MDCT = 0.1 mSv)[11]. Wrist and Ankle 4DCT radiation doses are also within a similar range of up to 1 mSv, comparable to the measured doses for 4DCT acquisition of other peripheral joints[12]. Skin is the only radiation-sensitive tissue in the field-of-view of a peripheral joint 4DCT. Therefore, the extremity conversion factors are fairly low (e.g., 0.005 and 0.001 for the knee and other peripheral joints, respectively)[13]. Consequently, even for 4D scans with a marked increase in cumulative radiation exposure, the effective radiation doses are lower than in common single-acquistion MDCT acquisition sites in routine clinical practice such as head & neck, chest, or abdomen[13]. Regardless, as future innovations become more integrated with clinical practice, CT scanner vendors are implored to make available the information required to make accurate dosimetric measurements in order to properly estimate cancer risks[14].

Knee imaging

4DCT of the knee is helpful in the characterization of biomechanical derangements of the patellofemoral joint with specific efforts on elucidating the relationship between patellofemoral instability and patellofemoral maltracking. Traditional evaluation of patellofemoral maltracking is performed during physical examination through detection of acute lateral translation of the patella during terminal extension, also known as the “J sign”[15].

A prior study conducted 4DCT assessment of patients with patellofemoral instability, demonstrating a high prevalence of abnormal tracking patterns in both symptomatic and asymptomatic knees of such patients and higher still for only symptomatic knees (i.e., anterior knee pain and stiffness; catching or buckling of the knee on movement, and recurrent chronic dislocations, regardless of surgical intervention)[16]. Moreover, the study used the acquired images to radiologically identify the J-sign and grade degrees of maltracking, revealing a positive correlation of higher grades of maltracking with symptomatic patellar instability in the presence of a radiographic J-sign[16].

4DCT acquisitions have also demonstrated the presence of abnormal patellofemoral morphological features in the contralateral asymptomatic knees of patients with unilateral patellofemoral instability compared to matched knee examinations of subjects with clinical indications other than patellofemoral pathologies (e.g., knee trauma). This includes decreased trochlear groove depth, higher tibial tuberosity-trochlear groove (TT-TG) distances, increased patellar height ratios, and increased patellar bisect offset at various angles of knee flexion in cases compared to controls[11]. This work also suggests that data obtained from both static and kinematic scans can be utilized to identify early patellofemoral osteoarthritis[11].

4DCT examinations have also shown higher TT-TG distance, lateral patellar tilt, and bisect offset measurements in unstable knees in patients with patellofemoral instability as opposed to the asymptomatic contralateral knee at various degrees of knee flexion. Decreasing trends in the measurements at increased levels of flexion were also observed, indicating that dynamic evaluation may improve the diagnostic accuracy[17].

Use of 4D CT can also be helpful in the evaluation of corrective patellofemoral surgery outcomes. For example, in one study of pre- and post-operative evaluation of individuals who have undergone medial patellofemoral ligament reconstruction, 4DCT confirmed successful patellar stabilization and was sensitive for the detection of residual patellar tilt and shift (Figure 1)[18].

The role of 4DCT in the knee also extends beyond the characterization of patellofemoral instability. 4DCT studies of the knee can also be used to study biomechanical derangements of the knee due to ligamentous and meniscal defects, as has been shown by its ability to demonstrate decreased external rotation of the tibia relative to the femur during extension (screw home movement) in patients with anterior cruciate ligament deficiency[19].

With such promising prospects for 4DCT, semi-automatic workflows have been described that allow computation of TT-TG and patellar center – trochlear groove distances during a flexion/extension motion, the former in agreement with manual observations[20]. Further studies to optimize workflow may further facilitate the implementation of 4DCT in clinical practice for the diagnosis and post-intervention evaluation of patellofemoral instability and other knee pathologies[21].

Foot and Ankle Imaging

The structural and kinematic complexity of the ankle joint and its possible associated biomechanical derangements may benefit greatly from 4DCT evaluations, especially in place of unreliable clinical maneuvers and 2D radiographic measurements currently employed for pathologies like syndesmotic injuries[22].

An initial study outlining baseline measurements of five characteristics (syndesmotic anterior and posterior distances, syndesmotic translation, syndesmotic tibiofibular angle, and ankle tibiofibular angle) of the tibiofibular syndesmosis in asymptomatic ankles of patients with unilateral ankle instability revealed a significant difference in syndesmotic translation values between maximal dorsiflexion and maximal plantarflexion[22]. A study conducted on asymptomatic ankles of patients with unilateral instability under the same dorsiflexion/plantarflexion motion also revealed external rotation of the fibula, in addition to changes in syndesmotic widths[23]. As more studies begin to outline the behavior of the joint in motion under both physiological and pathological conditions, reliable quantitative assessments in 4DCT can be a promising modality for the diagnosis and optimal characterization of syndesmotic injury.

In attempting to address a similar conundrum of unreliable diagnostics, physiological measurements of the subtalar joint have been conducted by Teixeira et al[24]. A subsequent comparative study of subtalar joints during pronosupination using 4DCT between healthy individuals and patients with joint stiffness and/or chronic ankle instability showed significantly decreased measurements of coronal and axial talocalcaneal angles in stiff joints, and decreased maximal posterior calcaneal facet uncovering in unstable joints[25].

Wrist Imaging

Like the ankle, the wrist is a mechanically complex joint, providing another potential opportunity to apply 4DCT in clinical practice. A common etiology for carpal instability is scapholunate interosseous ligament (SLIL) injury and insufficiency, which is traditionally studied using plain radiographs, 2D cineradiography, and clinical maneuvers initially before considering CT, MRI, and arthroscopy[26]. 2D modalities may fail to capture the intricate movements of the joints, and invasive measures are often undesirable, hence an emphasis on 3D imaging techniques should be made. 4DCT has been demonstrated as a plausible alternative in comparing asymptomatic and symptomatic wrists during three predefined motions (relaxed to clenched fist, flexion/extension, and radial/ulnar deviation)[27]. In this study, the average scapholunate interval changes in asymptomatic wrists were measured at < 1mm throughout all motions contrasting an average interval of >2mm in symptomatic wrists with clinical suspicion of SLIL insufficiency. Furthermore, a mild/moderate correlation was observed between SL interval changes and the presence of symptoms[27]. The prospective ACTION trial has been recently designed with the primary aim of establishing the role that 4DCT may be able to play in the diagnosis of scapholunate ligament injuries. It is in the process of prospective enrollment at the time of writing and will be a study of 120 (80 historical) patients scheduled for arthroscopy[28].

The biomechanics of the wrist pre- and post-operatively has also been assessed using 4DCT in a population of patients who underwent scapholunate ligament repair. The modality was able to consistently demonstrate dynamic ulnocarpal abutment in patients presenting with diffuse wrist pain and demonstrate adequate repair and kinematic stability in patients with a normal post-operative course[29].

Akin to SLIL assessment, wrists of patients experiencing ulnar-sided pain were diagnosed with pisotriquetral instability (PTI) using 4DCT in a recent case-series[30]. PTI is an uncommon etiology for medial wrist biomechanical derangement and has been traditionally evaluated using cineradiography[31]. Using 4DCT, abnormal volar subluxation of the pisiform was described in one patient with suspected PTI and medial wrist pain, whereas proximal subluxation of pisiform was observed in another patient with a chronic “clicking” sensation. Dynamic evaluation of the minimum anteroposterior pisotriquetral interval and proximal/distal translation of the pisiform in relation to the triquetrum over 11 measurements proved helpful in detecting subtle PTI in each case, respectively[30].

Other wrist pathologies of the wrist investigated using 4DCT include the Madelung deformity, which involves decreased lunate and triquetral motion[32], trigger lunate syndrome, consisting of cessation and subsequent catch-up of the lunate[33], and Kienböck’s disease, whereby disruption of blood supply results in lunate osteonecrosis[34].

To further establish the role of 4DCT in routine practice, several studies have been conducted to establish the normal range of motion of various small joints in the wrist according to predefined motions and 4DCT acquisition protocols. Alignment measurements of the asymptomatic distal radioulnar joints of patients using the modified radioulnar line and epicenter methods in a pronation-supination motion demonstrated that the former method can detect volar/dorsal motions of the ulnar head with excellent interobserver reliability[35]. The normal motion of the pisotriquetral joint during wrist flexion/extension, with measurements of the anteroposterior interval and craniocaudal excursion, have also been described with good interobserver agreement of the first measurement[31]. Recent quantification of scaphoid, lunate, and capitate motions in healthy individuals by using 4DCT have also been reported, with high test-retest reliability correlations[36]. Similar studies have also been conducted on varying wrist motion such as during radioulnar deviation, pronosupination[37].

Elbow, Hip, and Shoulder Joint Imaging

Elbow joint 4DCT has aided in the classification of traditionally clinically diagnosed entities such as bicipital impingement and osteoarthritis and complex diseases such as hemimelia and post open reduction/internal fixation implant impingements of the radial head and capitulum radii[38].

Due to the increased cumulative radiation exposures in 4DCT studies compared to conventional single-acquisition MDCT, more proximal joints of the human body, such as the hip and shoulder, are in close vicinity to radiation sensitive organs such as the thyroid and reproductive organs are usually used, not ideal sites for kinematic evaluation using 4DCT. Despite such potential concerns for radiation safety, studies have outlined the potential value

of 4DCT in the visualization of cam and pincer types of femoroacetabular impingement and associated subluxation[39]. Physiological movement of the acromioclavicular joint during adduction of the arm in loaded and unloaded states and the diagnosis of sternoclavicular joint instability have also been described using kinematic 4DCT acquisitions[40,41]. Scapular examinations have been used to detail dynamic impingement in patients with snapping scapula syndrome[42].

At our institution, we have refrained from studies of the proximal joints using 4DCT due to radiation exposure concerns. However, with newer radiation-reducing protocols and dose-reduction algorithms using artificial intelligence[43], we may revisit the potential application of 4DCT in assessing biomechanical derangements of proximal joints such as the hip and shoulder.

Cone Beam Computed Tomography

Cone Beam CT (CBCT) refers to a constellation of CT systems that use pyramidally-shaped x-ray beams with sufficient longitudinal width to permit imaging of entire organs in a single gantry rotation using large-area flat-panel detectors (FPDs)[44]. Such a wide axial coverage is becoming increasingly commonplace in MDCT technology and its application in routine clinical practice. In musculoskeletal imaging, the adoption of FPD-based CBCT has yielded a new diagnostic capability - weight-bearing (WB) volumetric imaging of the lower extremity[45]. In WB-CBCT, the x-ray source (typically a lightweight, low-power, fixed-anode x-ray tube) and the FPD rotate in a plane parallel to the floor with the examinee standing inside the gantry. Some WB-CBCT designs permit imaging of unloaded extremities of a seated subject by rotating the gantry into a vertical orientation. Ongoing development of fully robotized x-ray imaging rooms[46] may enable complex acquisition orbits for specialized musculoskeletal applications in the future, for example, WB spine imaging[47], metal artifact reduction[48,49], and improved dose efficiency during WB spine, foot and ankle CBCT acquisitions[50].

Below we review some of the image quality challenges specific to the application of CBCT for musculoskeletal imaging, the ongoing development of its capabilities, and the emerging clinical applications of WB volumetric imaging.

Motion Artifact Compensation

The technical features of FPD-CBCT that make it well suited for compact, application-specific 3D imaging platforms come at a price of several unique image quality challenges. For example, a relatively long acquisition time, typically on the order of >15 sec, render it prone to motion artifacts. New CBCT hardware show promise in addressing this issue by enabling rapid imaging[51,52]. Nevertheless, supplemental motion mitigation and compensation strategies will remain essential for the widespread utilization of CBCT in the foreseeable future.

Patient movement in CBCT can be somewhat mitigated by light immobilization. However, even in a closed-bore extremity WB-CBCT that permits relatively easy application of restraining cushions, moderate to severe motion artifacts have been observed[53].

Consequently, there is a need for compensation algorithms, whose development is made challenging by the aperiodic nature of patient movement in musculoskeletal CBCT (unlike cardiac or respiratory motions) that precludes the use of gating. Therefore, most compensation algorithms applicable to musculoskeletal CBCT first estimate the patient displacement in each projection view, usually assuming only rigid transformations. This estimate is then applied to modify each view's projection geometry during the back-projection step of image reconstruction.

A variety of motion estimation algorithms have been proposed. One category utilizes 3D-2D registration, which finds a sequence of spatial transformations that best map a known reference object present in the field-of-view (FOV) onto the measured projections. Possible choices of the reference object include skin-attached fiducials[54], prior motion-free scans of the same anatomy[55,56], and outlines of high-attenuation structures in the motion-contaminated scan[57]. The first two approaches suffer from workflow limitations (placement of the fiducials or availability of a prior scan), whereas the last might be suboptimal in addressing severe motions. Alternative methods rely on projection or image quality metrics to estimate the motion without 3D-2D registration. These include the application of projection consistency conditions[58,59] and image-based autofocus[53,60], the latter showing applicability to musculoskeletal CBCT.

In the autofocus approach, the compensation is achieved by performing numerical optimization to estimate a movement trajectory that minimizes some metric of image-domain distortion induced by motion; in musculoskeletal CBCT, the variance of image gradient was used as the metric[53,60]. In an expert observer study involving motion-contaminated extremity CBCT scans, the autofocus-corrected volumes exhibited improved diagnostic quality (Figure 2)[53].

Regional application of autofocus motion compensation enables individual estimation and correction of the movement of each bone in a joint. Extension of this approach to deformable soft-tissue motion compensation has been proven feasible by performing spatiotemporal interpolation between individual ROIs[61]. A deep-learning-based, reference-free version of the Visual Information Fidelity criterion was recently proposed to develop robust image distortion metrics that guard against local minima or degenerate motion estimates[62].

Foot and Ankle Imaging

An accurate and timely diagnosis of syndesmotic injuries is paramount in preventing chronic ankle instability and prevention of secondary osteoarthritis[22]. Conventional CT studies have analyzed the distal tibiofibular joint under non-weight-bearing conditions. As previously described, WB-CBCT helps supplement the diagnostic yields of non-weight-bearing examinations; however, the importance of the former has yet to be elucidated. In asymptomatic uninjured ankles, it has been shown that apart from the medial clear space, WB studies seem to have no discernible differences in syndesmotic measurements[63]. Conversely, in those with prior ankle injuries with clinical suspicion of syndesmotic injuries, there were differences between the measurements of the mean posterior tibiofibular distance, diastasis, and angular measurements between non-weight-bearing and WB studies with

interobserver reliability approaching near-perfect levels[64]. Injured ankles of patients with unilateral syndesmotic instability showed increased 3D volumetric WB-CBCT measurement values compared to the contralateral uninjured ankle at various levels proximal to the tibial plafond; such a difference was absent in healthy controls(Figure 3)[65].

3D WB-CBCT efficiently characterizes valgus hindfoot alignments in patients with adult acquired flatfoot deformity (AAFD) (Figure 4). Various radiological measurements for hindfoot alignment have been adopted from plain radiography and validated in 3D WB/non-weight-bearing CBCT images[63]. These measurements, including radiologically measured hindfoot alignment angle and Achilles' tendon/calcaneal tuberosity angle, have significantly differed from the mean of clinically measured hindfoot alignment angles[66]. The latter underestimated radiological assessments of valgus alignment by 10° to 15°, suggesting higher degrees of accuracy using CBCT instead of physical measurements[66]. Differences in measurements between WB and non-weight-bearing studies of AAFD have also been noted, the most reliable of which include medial cuneiform-to-floor distance, coronal forefoot arch angle, sagittal cuboid-to-floor distance, and sagittal navicular-to-floor distance (Figure 5)[67]. Additionally, measurements such as medial cuneiform-to-floor distance, navicular-to-floor distance, parasagittal talus-first-metatarsal-angle and medial-cuneiform-first-metatarsal-angle were shown be significantly different between WB radiographs and WB-CBCT[68].

Considering the complexity of the volumetric information provided by WB-CBCT, widespread adoption of quantitative metrics of 3D joint alignment will likely rely on automated measurement tools to improve the reliability of the human reader. Proposed solutions range from approaches that require manual selection of anatomical landmarks[69] to algorithms based on fitting a computer model of the ankle for detecting the landmarks automatically[70,71]. In the future, quantitative evaluation of foot and ankle CBCT will likely expand beyond the point-to-point metrics described here to include comprehensive analysis of morphological variations in the population using statistical shape models[72].

Knee Imaging

CBCT can also be helpful in certain knee pathologies that accentuate during weight-bearing. The effects of varying time-lengths of weight-bearing on knee cartilage and meniscal movement, detection of cartilage and subchondral bone abnormalities in posttraumatic arthritic knees, and patellofemoral and tibiofemoral alignment in weight-bearing and supine positions have all been the object of recent studies[73–75]. In addition to weight-bearing capability, volumetric bone mineral density (vBMD) evaluation of knee subchondral bone can be performed using CBCT like quantitative CT. A combined cadaveric/live subject study[76] showed high vBMD correlations between CBCT and CT, although there were differences in absolute values between scanners.

In addition to bone mineral density, contrast-enhanced CBCT may also prove useful in assessing cartilage thickness and distribution. Cartilage thickness methodologies applied to such examinations showed agreement in predicting tibial cartilage thickness distribution[77].

As in foot and ankle imaging, knee CBCT benefits from automated methods for identifying anatomical landmarks and measurements, including TT-TG distance, medial and lateral tibial slopes, and medial tibial depth, to improve accuracy and reliability and pace of data gathering using the large volumetric datasets. To this end, an approach where landmarks identified by expert readers in an atlas set of CBCT scans were transported onto the target volumes using image registration has been described[78]. Such methods may prove invaluable in providing consistent interpretations in clinical practice and aid in detecting subtle biomechanical derangements during physiological weight-bearing. Application of statistical shape models derived from the CBCT volumes[79] might augment such point-to-point measurements by providing quantitative insights into morphological variability of the knee joint.

Compared to traditional MDCT, the high isotropic spatial resolutions and lower effective radiation doses offered by CBCT for soft-tissue imaging have a high potential to be sensitive to subtle changes in joint space morphology encountered in osteoarthritis and related conditions. Moreover, with advanced image post-processing, CBCT has demonstrated strong correlations with gold standard micro-CT in measurements of trabecular microstructure[80]. In its ability to simultaneously obtain bone vBMD and microstructural quality measures, CBCT might provide a useful adjunct to pre-clinical imaging using high-resolution peripheral quantitative CT (HR-pQCT), with the benefit of being readily applicable to larger joints. However, in comparison to HR-pQCT, CBCT tends to overestimate trabecular parameters and underestimate cortical parameters despite demonstrating overall bone architecture assessment feasibility[81].

Additionally, CBCT has been used to characterize tibiofemoral joint space morphology by generating spatial maps of local joint space width (JSW) across the entire articular surface of the tibia (or, equivalently, the femur)[82]. For example, an electrostatic model that can provide quantitative assessments of JSW was shown to perform on par with a radiologist reading for minimal joint space width in the medial compartment with improved performance after principal component analysis[82]. CBCT has also been used to describe medial tibiofemoral joint space width reduction and meniscal extrusion, which accentuate during WB-CBCT acquisition compared to non-weight-bearing examinations in patients with knee osteoarthritis; such biomechanical derangements were insignificant in healthy controls[83]. Focal cartilage lesions and their effect on contact mechanics of the knee joint, a relationship with proven progression to osteoarthritis if left uncorrected, have also been described to a high level of detail using CBCT studies[84].

Trauma and Fracture Imaging

CBCT arthrography has shown significant success in the detection of cartilage defects. In shoulder arthrography, different CBCT acquisition protocols have shown a trade-off between radiation dose and sensitivity for rotator cuff and cartilage pathologies compared to traditional MDCT[85]. In addition, CBCT-arthrography protocols have shown better contrast-to-noise ratios and small structure spatial resolutions, showing potential for tailored protocols for cartilage evaluation[86]. In comparison to 1.5 T MRI, CBCT-arthrography has shown superior diagnostic performance in ankle cartilage defect detection in one study[87].

CBCT studies comparing its ability to detect fractures compared to plain radiographs, including those of the wrist, hand, finger, ankle, foot, and toe, demonstrated a remarkable improvement in sensitivity for detecting subtle fractures[88]. There is also an increase in the agreement of the advised orthopedic therapy due to CBCT interpretation from moderate to near perfect[88]. Similarly, increased sensitivity and detection rates (in comparison to plain radiographs) for wrist fractures have been observed using the modality[89]. A considerable pooled sensitivity and a high pooled specificity to detect and rule out scaphoid fractures using CBCT were found in a 2021 meta-analysis[90]. Excellent agreement with MDCT for distal extremity fractures has been reported, proving particularly advantageous when combined with better tolerance and lower effective radiation dose provided by CBCT[91].

In addition to imaging trauma and fracture in extremities, CBCT has been used intraoperatively to aid vertebral body stentoplasty, kyphoplasty, and vertebroplasty[92] and repair isolated displaced talar fractures[93], displaced acetabular fractures[94], and tibial plafond fractures[95]. Recent advancements show feasibility of field-of-view expansion of CBCT scans, enabling visualization of long anatomical sites intraoperatively[96]. In orthodontics and maxillofacial surgery, CBCT has not only been described extensively as a modality to aid in the diagnosis of skeletal defects of the skull and teeth but is also under study for evaluation of bone healing[97]. In addition, use of CBCT in the detection of medication-related osteonecrosis of the jaw are also reported, comparable to ultrashort echo-time MRI[98,99]. In conjunction with bone healing, studies are now being conducted to evaluate extremity joints with and without the presence of metal hardware[100].

Dual-Energy Computed Tomography

Dual-energy computed tomography (DECT) uses either two orthogonally placed rows of detectors or a single row of detectors with alternating voltages (conducted sequentially, or with the use of fast kilovoltage switching) to acquire two independent data sets at two different levels of voltage peaks[101]. A retrospective acquisition technique also uses a layered detector approach, partitioning low- and high-energy photons and simultaneously acquiring both datasets as with dual-source DECT[101].

A meta-analysis exploring the sensitivity of DECT in detecting bone marrow edema (BME) in vertebral body fractures notes the advantage of single-source consecutive scanning because of lower logistical requirements that leads to better availability[102]. However, poor co-registration becomes evident in such techniques, leading to decreased specificities compared to other DECT techniques[102].

Reconstructed CT images undergo post-processing algorithms specializing in image optimization, material-specific display, and substance quantification[101]. Numerous image types can be achieved, including weighted average, monoenergetic, and virtual suppression images and electron density and atomic number maps[103,104]. In musculoskeletal imaging, DECT-based virtual subtraction permits studying soft-tissue structures accurately, which is particularly useful in acute care settings[103].

Trauma Imaging

Radiographically occult and subtle fractures are important to detect early to prevent and reduce the risk of significant morbidity. The traditional evaluation of such suspected fractures is done through MRI. However, DECT plays a key role in triaging patients in acute trauma settings.

As discussed before, the emerging role of DECT in detecting BME using virtual non-calcium (VNC) maps has shown excellent diagnostic performance[105]. In current literature, VNC-DECT has shown comparable (and in some cases, superior) sensitivity and specificity to MRI in detecting BME and acute fracture lines in the setting of spine[106,107], knee[108], ankle[109], pelvic ring[110], and wrist[111] trauma. Preliminary studies suggest the usefulness of contrast enhanced DECT in predicting avascular necrosis after proximal humerus fractures[112].

Material decomposition algorithms applied to DECT could prove useful in detecting iron-containing debris in cases of penetrating injuries, whereas the metal artifact reduction capabilities of DECT (particularly beam-hardening artifacts) that can improve delineation of the surrounding tissues[103]. Such an advantage is also useful in studying patients with metallic prostheses. Indeed, virtual monochromatic DECT has improved the evaluation of suspected appendicular skeleton non-union treated with intramedullary nails and plates[113].

Gout and Rheumatological Imaging

An intriguing use of DECT is diagnosing gout using both multiplanar and 3D material decomposition reconstructions[114], analogous to differentiating uric acid nephrolithiasis from other kidney stone compositions (Figure 6). A recent meta-analysis shows a higher pooled sensitivity and specificity to detect gout using DECT than ultrasound for more than two years of disease duration[115].

Recent efforts to distinguish crystal deposition types were successful in differentiating monosodium urate deposits (prevalent in gout) from calcium pyrophosphate (prevalent in pseudogout) or calcium hydroxyapatite deposits in a phantom study[116].Similarly, an exploration of varying DECT decomposition methods demonstrated the utility of 3D virtual monochromatic acquisitions in quantification and detection of monosodium urate deposits in a phantom-controlled study of subjects' feet and ankles[117].

Limitations of DECT in diagnosing gout have also been described in current literature. DECT does not perform as well as ultrasound in patients in the early stage of the disease[115]. Low sensitivity has been reported for DECT in detecting gout in patients with symptom duration less than six weeks[118] and non-tophaceous gout[119]. DECT has also shown to have limited detection of urate in patient-derived liquid tophi due to subthreshold attenuation[120].

There is an emerging interest in the capabilities of DECT in other rheumatological entities as well. VNC-DECT has shown to have excellent diagnostic performance in the detection of bone marrow edema in sacroiliac joints of patients with suspected axial spondyloarthritis, with substantial interreader agreeability on lesion grading[121].

Neoplasm Imaging

DECT also has an emerging role in detecting neoplasms of the bone marrow. Both primary and metastatic lesions have been described in the literature as having benefitted from a DECT examination. VNC-DECT imaging has shown high accuracy in detecting bone marrow infiltration in patients with multiple myeloma and monoclonal gammopathy of unknown significance[122]. With careful region-of-interest selection, significant differences have been described in mean VNC-DECT attenuation levels for different patterns of plasma cell disorders[123]. Testing the sensitivity of VNC-DECT revealed that the detection of non-osteolytic infiltration was better than traditional CT but lower than MRI for moderately infiltrating lesions[124].

Dual-Energy Cone Beam Computed Tomography

DE techniques can be implemented in CBCT following principles like those employed in conventional CT. However, the CBCT technology poses certain unique challenges, some of which are related to scanner hardware. For instance, rapid tube potential switching between consecutive views, known from conventional DECT, might be difficult to realize in CBCT because of x-ray tube limitations, relatively slow FPD frame rates, and FPD lag between exposures. Furthermore, CBCT is more susceptible to artifacts, elevated scatter-to-primary ratios (due to the large detector area) and diminished contrast-to-noise ratios (partly due to relatively high electronic noise in FPDs) than conventional CT. DE material decomposition is highly sensitive to such non-idealities. Therefore, robust DE-CBCT imaging requires continuing development of accurate artifact corrections and noise reduction strategies[125,126].

Despite these challenges, initial results of studies implementing DE-CBCT show promise. A possible practical realization of DE-CBCT on a dedicated musculoskeletal scanner has been reported using the Carestream OnSight system[127], which provides a unique multi-source x-ray unit with three x-ray tubes arranged longitudinally along the scan rotation axis, improving upon the clinically impractical sequential configurations described in preliminary feasibility studies[128]. In addition to such specialized source-side designs, it is likely that multi-layer FPDs[129] will be implemented in musculoskeletal CBCT in the near future, similar to the layered detector systems for conventional DECT. Initial imaging physics performance evaluation studies of multi-layer FPDs in DE-CBCT confirmed near-perfect accuracy in measurements of atomic number and electron density[130] and few errors in calcium and iodine concentration measurements[129].

The formation of material concentration images in DE-CBCT has been reported using all major categories of computational approaches known from DECT: pre-reconstruction projection-domain decomposition (PDD)[126], post-reconstruction image-domain decomposition (IDD)[131], and direct iterative one-step model-based material decomposition (MBMD)[132]. MBMD has the potential to achieve improved resolution-noise tradeoff compared to analytical methods and the ability to incorporate prior knowledge – for example, metal hardware models present in the FOV, enabling DE imaging around orthopedic hardware[132].

Intraarticular Contrast-Enhanced Imaging

DE-CBCT can potentially aid the discrimination of intraarticular contrast agents from the neighboring bone, as was investigated in phantom and cadaver studies using an investigational dual-scan DE protocol and post-reconstruction image-domain decomposition[131]. For larger detail sizes, high iodine detection accuracy was found for analytical and model-based reconstruction algorithms at imaging doses of 10 mGy or less; at ~15 mGy, iodine details as small as ~3 mm were classified with great accuracy using model-based reconstruction with edge-preserving regularization. Future applications of DE-CBCT in arthrography might be extended to recently proposed multi-contrast protocols for CT-based assessment of cartilage[133]. In this technique, proteoglycan distribution in cartilage is quantified using the cationic agent, and the water distribution is revealed using the non-ionic agent.

Bone Densitometry

Application of DE-CBCT to BMD evaluation has recently been reported in dental imaging[134]. In musculoskeletal imaging, a simulation study assuming perfect scatter correction found an accurate assessment of BMD by DE-CBCT[132]; with low-error measurements even in the vicinity of metal hardware when a prior model of the hardware was included in the MBMD. However, accurate scatter correction will likely be essential for robust BMD estimation using DE-CBCT[126].

Bone Marrow Imaging

Early feasibility studies of bone marrow lesion detection in DE-CBCT have been reported. The primary challenge in this application is the poor spectral separation between fat and water (edema fluid). Physical experiments emulating the three-source extremity CBCT mentioned earlier showed that a DE technique can readily distinguish fat (simulated by ethyl alcohol) from the water-like plastic in a bone densitometry insert; simulation studies further demonstrated that high accuracy in the detection of fluid collection within trabecular bone might be achieved with DE-CBCT assuming adequate scatter correction (Figure 7)[127]. Evidence from a recent computer modeling of a hypothetical DE-CBCT system based on a dual-layer FPD also indicated that BME detection in a knee-sized object is feasible[135].

Conclusion

Novel and evolving 4DCT, CBCT, and DECT techniques contribute to the early and robust characterization of various musculoskeletal abnormalities. While MRI provides superior visualization due to its higher spatial resolution, tremendous opportunities exist for novel CT techniques. Kinematic analysis using 4DCT provides valuable information on abnormal motion and underlying biomechanical derangement of peripheral joints, aiding in diagnosing otherwise “occult” disorders and providing valuable information on the post-intervention outcomes. CBCT enables the analysis of musculoskeletal conditions during physiological weight-bearing and has found a role in intraoperative imaging, trauma imaging, and bone healing assessment. The ability to produce images with virtually removed calcium densities makes DECT an excellent tool for detecting bone marrow abnormalities. Applications include diagnosing bone marrow abnormalities in traumatic and non-traumatic

settings, ranging from diagnosing radiographically occult fractures to the classification of metastatic and primary bone marrow neoplasms. The ability of DECT to study crystal arthropathies can also play a crucial role in clinical practice, where it performs better than radiography. Finally, the emerging application of DE techniques to CBCT will further enhance the functionality of CT technologies in intraarticular contrast discrimination, BMD quantification, and BME detection, layering the benefit of DE and CBCT together.

References

1. Shakoor D, Kijowski R, Guermazi A, et al. Diagnosis of Knee Meniscal Injuries by Using Three-dimensional MRI: A Systematic Review and Meta-Analysis of Diagnostic Performance. Radiology. 2019;290(2):435–445. doi:10.1148/radiol.2018181212. [PubMed: 30457479]
2. Shakoor D, Guermazi A, Kijowski R, et al. Diagnostic Performance of Three-dimensional MRI for Depicting Cartilage Defects in the Knee: A Meta-Analysis. Radiology. 2018;289(1):71–82. doi:10.1148/radiol.2018180426. [PubMed: 30015587]
3. Fritz J, Raithel E, Thawait GK, et al. Six-fold acceleration of high-spatial resolution 3D SPACE MRI of the knee through incoherent k-space undersampling and iterative reconstruction - First experience. Invest Radiol. 2016;51(6):400–409. doi:10.1097/RLI.0000000000000240. [PubMed: 26685106]
4. Fritz J, Fritz B, Thawait GG, et al. Three-Dimensional CAIPIRINHA SPACE TSE for 5-Minute High-Resolution MRI of the Knee. Invest Radiol. 2016;51(10):609–617. doi:10.1097/RLI.0000000000000287. [PubMed: 27187045]
5. Khodarahmi I, Fritz J. The Value of 3 Tesla Field Strength for Musculoskeletal Magnetic Resonance Imaging. Invest Radiol. 2021;56(11):749–763. doi:10.1097/RLI.0000000000000801. [PubMed: 34190717]
6. del Grande F, Guggenberger R, Fritz J. Rapid musculoskeletal MRI in 2021: Value and optimized use of widely accessible techniques. AJR Am J Roentgenol. 2021;216(3):704–717. doi:10.2214/AJR.20.22901. [PubMed: 33534619]
7. Alkadhi H, Euler A. The Future of Computed Tomography: Personalized, Functional, and Precise. Invest Radiol. 2020;55(9):545–555. doi:10.1097/RLI.0000000000000668. [PubMed: 32209817]
8. Burrill J, Dabbagh Z, Gollub F, et al. Multidetector computed tomographic angiography of the cardiovascular system. Postgrad Med J. 2007;83(985):698–704. doi:10.1136/pgmj.2007.061804. [PubMed: 17989269]
9. Santoso AP, Song KH, Qin Y, et al. Evaluation of gantry speed on image quality and imaging dose for 4D cone-beam CT acquisition. Radiat Oncol. 2016;11(1):98. doi:10.1186/s13014-016-0677-8. [PubMed: 27473367]
10. Noid G, Tai A, Chen G-P, et al. Reducing radiation dose and enhancing imaging quality of 4DCT for radiation therapy using iterative reconstruction algorithms. Adv Radiat Oncol. 2017;2(3):515–521. doi:10.1016/j.adro.2017.04.003. [PubMed: 29114620]
11. Demehri S, Thawait GK, Williams AA, et al. Imaging characteristics of contralateral asymptomatic patellofemoral joints in patients with unilateral instability. Radiology. 2014;273(3):821–830. doi:10.1148/radiol.14140295. [PubMed: 25153158]
12. Demehri S, Chalian M, Farahani SJ, et al. Detection and Characterization of Tendon Abnormalities With Multidetector Computed Tomography. J Comput Assist Tomogr. 2014. doi:10.1097/RCT.0b013e3182aa72bf.
13. Mettler FAJ, Huda W, Yoshizumi TT, et al. Effective doses in radiology and diagnostic nuclear medicine: a catalog. Radiology. 2008;248(1):254–263. doi:10.1148/radiol.2481071451. [PubMed: 18566177]
14. Damilakis J. CT Dosimetry: What Has Been Achieved and What Remains to Be Done. Invest Radiol 2021;56(1):62–68. doi:10.1097/RLI.0000000000000727. [PubMed: 32932380]
15. Hadidi O, Ellanti P, Lincoln M, et al. The J-sign in patellar maltracking. BMJ Case Rep. 2018; 2018:bcr2017222887. doi: 10.1136/bcr-2017-222887.

16. Tanaka MJ, Elias JJ, Williams AA, et al. Characterization of patellar maltracking using dynamic kinematic CT imaging in patients with patellar instability. Knee Surg Sports Traumatol Arthrosc. 2016;24(11):3634–3641. doi: 10.1007/s00167-016-4216-9. [PubMed: 27358051]
17. Williams AA, Elias JJ, Tanaka MJ, et al. The Relationship Between Tibial Tuberosity-Trochlear Groove Distance and Abnormal Patellar Tracking in Patients With Unilateral Patellar Instability. Arthroscopy. 2016;32(1):55–61. doi: 10.1016/j.arthro.2015.06.037. [PubMed: 26440373]
18. Gobbi RG, Demange MK, de Ávila LFR, et al. Patellar tracking after isolated medial patellofemoral ligament reconstruction: dynamic evaluation using computed tomography. Knee Surg Sports Traumatol Arthrosc. 2017;25(10):3197–3205. doi: 10.1007/s00167-016-4284-x. [PubMed: 27544273]
19. Morishige Y, Harato K, Oki S, et al. Four-dimensional computed tomographic analysis of screw home movement in patients with anterior cruciate ligament deficient knee - a 3D-3D registration technique. Skeletal Radiol. 2022. doi: 10.1007/s00256-021-03986-3.
20. Chen H, Kluijtmans L, Bakker M, et al. A robust and semi-automatic quantitative measurement of patellofemoral instability based on four dimensional computed tomography. Med Eng Phys. 2020;78:29–38. doi: 10.1016/j.medengphy.2020.01.012. [PubMed: 32115353]
21. Forsberg D, Lindblom M, Quick P, et al. Quantitative analysis of the patellofemoral motion pattern using semi-automatic processing of 4D CT data. Int J Comput Assist Radiol Surg. 2016;11(9):1731–1741. doi: 10.1007/s11548-016-1357-8. [PubMed: 26932337]
22. Mousavian A, Shakoor D, Hafezi-Nejad N, et al. Tibiofibular syndesmosis in asymptomatic ankles: initial kinematic analysis using four-dimensional CT. Clin Radiol. 2019;74(7):571.e1–571.e8. doi: 10.1016/j.crad.2019.03.015.
23. Wong MT, Wiens C, Lamothe J, et al. Four-Dimensional CT Analysis of Normal Syndesmotic Motion. Foot Ankle Int. 2021;42(11):1491–1501. doi: 10.1177/10711007211015204. [PubMed: 34088231]
24. Gondim Teixeira PA, Formery A-S, Jacquot A, et al. Quantitative Analysis of Subtalar Joint Motion With 4D CT: Proof of Concept With Cadaveric and Healthy Subject Evaluation. AJR Am J Roentgenol. 2017;208(1):150–158. doi: 10.2214/AJR.16.16434. [PubMed: 27809555]
25. Gondim Teixeira PA, Formery A-S, Balazuc G, et al. Comparison between subtalar joint quantitative kinematic 4-D CT parameters in healthy volunteers and patients with joint stiffness or chronic ankle instability: A preliminary study. Eur J Radiol. 2019;114:76–84. doi: 10.1016/j.ejrad.2019.03.001. [PubMed: 31005181]
26. Konopka G, Chim H. Optimal management of scapholunate ligament injuries. Orthop Res Rev. 2018;10:41–54. doi: 10.2147/ORR.S129620. [PubMed: 30774459]
27. Demehri S, Hafezi-Nejad N, Morelli JN, et al. Scapholunate kinematics of asymptomatic wrists in comparison with symptomatic contralateral wrists using four-dimensional CT examinations: initial clinical experience. Skeletal Radiol. 2016;45(4):437–446. doi: 10.1007/s00256-015-2308-0. [PubMed: 26659662]
28. Goelz L, Kim S, Güthoff C, et al. ACTION trial: a prospective study on diagnostic Accuracy of 4D CT for diagnosing Instable ScaphOlunate DissociatioN. BMC Musculoskelet Disord. 2021;22(1):84. doi: 10.1186/s12891-021-03946-x. [PubMed: 33451307]
29. Shores JT, Demehri S, Chhabra A. Kinematic “4 Dimensional” CT Imaging in the Assessment of Wrist Biomechanics Before and After Surgical Repair. Eplasty. 2013;13:e9. [PubMed: 23573338]
30. Demehri S, Wadhwa V, Thawait GK, et al. Dynamic evaluation of pisotriquetral instability using 4-dimensional computed tomography. J Comput Assist Tomogr. 2014;38(4):507–512. doi: 10.1097/RCT.0000000000000074. [PubMed: 24834894]
31. Demehri S, Hafezi-Nejad N, Thakur U, et al. Evaluation of pisotriquetral motion pattern using four-dimensional CT: initial clinical experience in asymptomatic wrists. Clin Radiol. 2015;70(12):1362–1369. doi: 10.1016/j.crad.2015.07.007. [PubMed: 26343445]
32. Peymani A, de Roo MGA, Dobbe JGG, et al. Carpal Kinematics in Madelung Deformity. J Hand Surg Am. 2021;46(7):622.e1–622.e12. doi: 10.1016/j.jhsa.2020.11.016.
33. Troupis JM, Amis B. Four-dimensional computed tomography and trigger lunate syndrome. J Comput Assist Tomogr. 2013;37(4):639–643. doi: 10.1097/RCT.0b013e31828b68ec. [PubMed: 23863544]

34. MacLean SBM, Bain GI. Kinematics of the wrist in Kienböck's disease: a four-dimensional computed tomography study. J Hand Surg Eur Vol. 2021;46(5):504–509. doi: 10.1177/1753193420987790. [PubMed: 33491570]
35. Shakoor D, Hafezi-Nejad N, Haj-Mirzaian A, et al. Kinematic Analysis of the Distal Radioulnar Joint in Asymptomatic Wrists Using 4-Dimensional Computed Tomography-Motion Pattern and Interreader Reliability. J Comput Assist Tomogr. 2019;43(3):392–398. doi: 10.1097/RCT.0000000000000839. [PubMed: 30762658]
36. Brinkhorst M, Foumani M, van Rosmalen J, et al. Quantifying in vivo scaphoid, lunate, and capitate kinematics using four-dimensional computed tomography. Skeletal Radiol. 2021;50(2):351–359. doi: 10.1007/s00256-020-03543-4. [PubMed: 32734373]
37. Neu CP, Crisco JJ, Wolfe SW. In vivo kinematic behavior of the radio-capitate joint during wrist flexion-extension and radio-ulnar deviation. J Biomech. 2001;34(11):1429–1438. doi: 10.1016/s0021-9290(01)00117-8. [PubMed: 11672717]
38. Seah RB, Mak W-K, Bryant K, et al. Four-dimensional computed tomography scan for dynamic elbow disorders: recommendations for clinical utility. JSES Int. 2021. doi: 10.1016/j.jseint.2021.09.013.
39. Wassilew GI, Janz V, Heller MO, et al. Real time visualization of femoroacetabular impingement and subluxation using 320-slice computed tomography. J Orthop Res. 2013;31(2):275–281. doi: 10.1002/jor.22224. [PubMed: 22961635]
40. Goh YP, Kamali Moaveni A, Hoy G, et al. Dynamic assessment of sternoclavicular joint instability using four-dimensional computed tomography. J Med Imaging Radiat Oncol. 2019;63(2):216–221. doi: 10.1111/1754-9485.12862. [PubMed: 30801943]
41. Alta TD, Bell SN, Troupis JM, et al. The new 4-dimensional computed tomographic scanner allows dynamic visualization and measurement of normal acromioclavicular joint motion in an unloaded and loaded condition. J Comput Assist Tomogr. 2012;36(6):749–754. doi: 10.1097/RCT.0b013e31826dbc50. [PubMed: 23192215]
42. Bell SN, Troupis JM, Miller D, et al. Four-dimensional computed tomography scans facilitate preoperative planning in snapping scapula syndrome. J Shoulder Elbow Surg. 2015;24(4):e83–90. doi: 10.1016/j.jse.2014.09.020. [PubMed: 25457777]
43. Seah J, Brady Z, Ewert K, et al. Artificial intelligence in medical imaging: implications for patient radiation safety. Br J Radiol. 2021;94(1126):20210406. doi: 10.1259/bjr.20210406. [PubMed: 33989035]
44. Siewerdsen JH. Cone-Beam CT Systems. In: Samei E, Pelc NJ, eds. Computed Tomography : Approaches, Applications, and Operations. Cham: Springer International Publishing; 2020:11–26. doi: 10.1007/978-3-030-26957-9_2
45. Carrino JA, Al Muhit A, Zbijewski W, et al. Dedicated Cone-Beam CT System for Extremity Imaging. Radiology. 2013;270(3):816–824. doi: 10.1148/radiol.13130225. [PubMed: 24475803]
46. Fieselmann A, Steinbrener J, Jerebko AK, et al. Twin robotic x-ray system for 2D radiographic and 3D cone-beam CT imaging. In: Proc.SPIE.Vol 9783. Published online March 22, 2016. doi: 10.1117/12.2212242
47. Benz RM, Harder D, Amsler F, et al. Initial Assessment of a Prototype 3D Cone-Beam Computed Tomography System for Imaging of the Lumbar Spine, Evaluating Human Cadaveric Specimens in the Upright Position. Invest Radiol. 2018;53(12):714–719. doi: 10.1097/RLI.0000000000000495. [PubMed: 30001256]
48. Wu P, Sheth N, Sisniega A, et al. C-arm orbits for metal artifact avoidance (MAA) in cone-beam CT. Phys Med Biol. 2020;65(16):165012. doi: 10.1088/1361-6560/ab9454. [PubMed: 32428891]
49. Thies M, Zäch J-N, Gao C, et al. A learning-based method for online adjustment of C-arm Cone-beam CT source trajectories for artifact avoidance. Int J Comput Assist Radiol Surg. 2020;15(11):1787–1796. doi: 10.1007/s11548-020-02249-1. [PubMed: 32840721]
50. Zhao C, Herbst M, Vogt S, et al. Cone-beam imaging with tilted rotation axis: Method and performance evaluation. Med Phys. 2020;47(8):3305–3320. doi: 10.1002/mp.14209. [PubMed: 32340069]

51. Cao Q, Sisniega A, Brehler M, et al. Modeling and evaluation of a high-resolution CMOS detector for cone-beam CT of the extremities. Med Phys. 2018;45(1):114–130. doi: 10.1002/mp.12654 [PubMed: 29095489]
52. Freestone S, Weisfield R, Tognina C, et al. Analysis of a new indium gallium zinc oxide (IGZO) detector. In: Proc.SPIE.Vol 11312. Published online March 16, 2020. doi: 10.1117/12.2549469
53. Sisniega A, Thawait GK, Shakoor D, et al. Motion compensation in extremity cone-beam computed tomography. Skeletal Radiol. 2019;48(12):1999–2007. doi: 10.1007/s00256-019-03241-w [PubMed: 31172206]
54. Choi J-H, Maier A, Keil A, et al. Fiducial marker-based correction for involuntary motion in weight-bearing C-arm CT scanning of knees. II. Experiment. Med Phys. 2014;41(6):61902. doi: 10.1118/1.4873675.
55. Berger M, Müller K, Aichert A, et al. Marker-free motion correction in weight-bearing cone-beam CT of the knee joint. Med Phys. 2016;43(3):1235–1248. doi: 10.1118/1.4941012. [PubMed: 26936708]
56. Ouadah S, Jacobson M, Stayman JW, et al. Correction of patient motion in cone-beam CT using 3D-2D registration. Phys Med Biol. 2017;62(23):8813–8831. doi: 10.1088/1361-6560/aa9254. [PubMed: 28994668]
57. Unberath M, Choi J-H, Berger M, et al. Image-based compensation for involuntary motion in weight-bearing C-arm cone-beam CT scanning of knees. In: Proc.SPIE.Vol 9413. Published online March 20, 2015. doi: 10.1117/12.2081559
58. Berger M, Xia Y, Aichinger W, et al. Motion compensation for cone-beam CT using Fourier consistency conditions. Phys Med Biol. 2017;62(17):7181–7215. doi: 10.1088/1361-6560/aa8129. [PubMed: 28741597]
59. Aichert A, Berger M, Wang J, et al. Epipolar Consistency in Transmission Imaging. IEEE Trans Med Imaging. 2015;34(11):2205–2219. doi: 10.1109/TMI.2015.2426417. [PubMed: 25915956]
60. Sisniega A, Stayman JW, Yorkston J, et al. Motion compensation in extremity cone-beam CT using a penalized image sharpness criterion. Phys Med Biol. 2017;62(9):3712–3734. doi: 10.1088/1361-6560/aa6869. [PubMed: 28327471]
61. Capostagno S, Sisniega A, Stayman JW, et al. Deformable motion compensation for interventional cone-beam CT. Phys Med Biol. 2021;66(5):55010. doi: 10.1088/1361-6560/abb16e.
62. Huang H, Siewerdsen J, Zbijweski W, et al. Reference-Free, Learning-Based Image Similarity: Application to Motion Compensation in Cone-Beam CT. Phys Med Biol. 2022. doi: 10.1088/1361-6560/ac749a.
63. Shakoor D, Osgood GM, Brehler M, et al. Cone-beam CT measurements of distal tibio-fibular syndesmosis in asymptomatic uninjured ankles: does weight-bearing matter? Skeletal Radiol. 2019;48(4):583–594. doi: 10.1007/s00256-018-3074-6. [PubMed: 30242446]
64. Osgood GM, Shakoor D, Orapin J, et al. Reliability of distal tibio-fibular syndesmotic instability measurements using weightbearing and non-weightbearing cone-beam CT. Foot Ankle Surg. 2019;25(6):771–781. doi: 10.1016/j.fas.2018.10.003. [PubMed: 30442425]
65. Bhimani R, Ashkani-Esfahani S, Lubberts B, et al. Utility of Volumetric Measurement via Weight-Bearing Computed Tomography Scan to Diagnose Syndesmotic Instability. Foot Ankle Int. 2020;41(7):859–865. doi: 10.1177/1071100720917682. [PubMed: 32419488]
66. de Cesar Netto C, Shakoor D, Roberts L, et al. Hindfoot alignment of adult acquired flatfoot deformity: A comparison of clinical assessment and weightbearing cone beam CT examinations. Foot Ankle Surg. 2019;25(6):790–797. doi: 10.1016/j.fas.2018.10.008. [PubMed: 30455094]
67. de Cesar Netto C, Schon LC, Thawait GK, et al. Flexible Adult Acquired Flatfoot Deformity: Comparison Between Weight-Bearing and Non-Weight-Bearing Measurements Using Cone-Beam Computed Tomography. J Bone Joint Surg Am. 2017;99(18):e98. doi: 10.2106/JBJS.16.01366. [PubMed: 28926392]
68. Shakoor D, de Cesar Netto C, Thawait GK, et al. Weight-bearing radiographs and cone-beam computed tomography examinations in adult acquired flatfoot deformity. Foot Ankle Surg. 2021;27(2):201–206. doi: 10.1016/j.fas.2020.04.011 [PubMed: 32475795]

69. Bernasconi A, Cooper L, Lyle S, et al. Intraobserver and interobserver reliability of cone beam weightbearing semi-automatic three-dimensional measurements in symptomatic pes cavovarus. Foot Ankle Surg. 2020;26(5):564–572. doi: 10.1016/j.fas.2019.07.005. [PubMed: 31378592]
70. Brehler M, Islam A, Vogelsang L, et al. Coupled Active Shape Models for Automated Segmentation and Landmark Localization in High-Resolution CT of the Foot and Ankle. Proc SPIE Int Soc Opt Eng. 2019;10953. doi: 10.1117/12.2515022.
71. Kvarda P, Heisler L, Krähenbühl N, et al. 3D Assessment in Posttraumatic Ankle Osteoarthritis. Foot Ankle Int. 2021; 42(2):200–214. doi: 10.1177/1071100720961315. [PubMed: 33073607]
72. Lenz AL, Krähenbühl N, Peterson AC, et al. Statistical shape modeling of the talocrural joint using a hybrid multi-articulation joint approach. Sci Rep. 2021;11(1):7314. doi: 10.1038/s41598-021-86567-7. [PubMed: 33795729]
73. Myller KAH, Turunen MJ, Honkanen JTJ, et al. In Vivo Contrast-Enhanced Cone Beam CT Provides Quantitative Information on Articular Cartilage and Subchondral Bone. Ann Biomed Eng. 2017;45(3):811–818. doi: 10.1007/s10439-016-1730-3. [PubMed: 27646147]
74. Hirschmann A, Buck FM, Fucentese SF, et al. Upright CT of the knee: the effect of weight-bearing on joint alignment. Eur Radiol. 2015;25(11):3398–3404. doi: 10.1007/s00330-015-3756-6. [PubMed: 25929941]
75. Halonen KS, Mononen ME, Jurvelin JS, et al. Deformation of articular cartilage during static loading of a knee joint--experimental and finite element analysis. J Biomech. 2014;47(10):2467–2474. doi: 10.1016/j.jbiomech.2014.04.013. [PubMed: 24813824]
76. Turunen MJ, Töyräs J, Kokkonen HT, et al. Quantitative evaluation of knee subchondral bone mineral density using cone beam computed tomography. IEEE Trans Med Imaging. 2015;34(10):2186–2190. doi: 10.1109/TMI.2015.2426684. [PubMed: 25935027]
77. Maier J, Black M, Bonaretti S, et al. Comparison of Different Approaches for Measuring Tibial Cartilage Thickness. J Integr Bioinform. 2017;14(2). doi: 10.1515/jib-2017-0015.
78. Brehler M, Thawait G, Kaplan J, et al. Atlas-based algorithm for automatic anatomical measurements in the knee. J Med Imaging (Bellingham). 2019;6(2):26002. doi: 10.1117/1.JMI.6.2.026002.
79. Charon N, Islam A, Zbijewski W. Landmark-free morphometric analysis of knee osteoarthritis using joint statistical models of bone shape and articular space variability. J Med Imaging (Bellingham). 2021;8(4):44001. doi: 10.1117/1.JMI.8.4.044001.
80. Brehler M, Cao Q, Moseley KF, et al. Robust Quantitative Assessment of Trabecular Microarchitecture in Extremity Cone-Beam CT Using Optimized Segmentation Algorithms. Proc SPIE Int Soc Opt Eng. 2018;10578. doi: 10.1117/12.2293346.
81. de Charry C, Boutroy S, Ellouz R, et al. Clinical cone beam computed tomography compared to high-resolution peripheral computed tomography in the assessment of distal radius bone. Osteoporos Int. 2016;27(10):3073–3082. doi: 10.1007/s00198-016-3609-4. [PubMed: 27121345]
82. Cao Q, Thawait G, Gang GJ, et al. Characterization of 3D joint space morphology using an electrostatic model (with application to osteoarthritis). Phys Med Biol. 2015;60(3):947–960. doi: 10.1088/0031-9155/60/3/947. [PubMed: 25575100]
83. Thawait GK, Demehri S, AlMuhit A, et al. Extremity cone-beam CT for evaluation of medial tibiofemoral osteoarthritis: Initial experience in imaging of the weight-bearing and non-weight-bearing knee. Eur J Radiol. 2015;84(12):2564–2570. doi: 10.1016/j.ejrad.2015.09.003. [PubMed: 26388464]
84. Venäläinen MS, Mononen ME, Salo J, et al. Quantitative Evaluation of the Mechanical Risks Caused by Focal Cartilage Defects in the Knee. Sci Rep. 2016;6:37538. doi: 10.1038/srep37538. [PubMed: 27897156]
85. Guggenberger R, Ulbrich EJ, Dietrich TJ, et al. C-arm flat-panel CT arthrography of the shoulder: Radiation dose considerations and preliminary data on diagnostic performance. Eur Radiol. 2017;27(2):454–463. doi: 10.1007/s00330-016-4382-7. [PubMed: 27221562]
86. Guggenberger R, Winklhofer S, Spiczak J v., et al. In vitro high-resolution flat-panel computed tomographic arthrography for artificial cartilage defect detection : Comparison With multidetector computed tomography. Invest Radiol. 2013;48(8):614–621. doi: 10.1097/RLI.0b013e318289fa78. [PubMed: 23538888]

87. Pagliano S, Chemouni D, Guggenberger R, et al. Flat-panel CT arthrography for cartilage defect detection in the ankle joint: first results in vivo. Skeletal Radiol. 2020;49(8):1259–1265. doi: 10.1007/s00256-020-03398-9. [PubMed: 32146486]

88. Grunz J-P, Pennig L, Fieber T, et al. Twin robotic x-ray system in small bone and joint trauma: impact of cone-beam computed tomography on treatment decisions. Eur Radiol. 2021;31(6):3600–3609. doi: 10.1007/s00330-020-07563-5 [PubMed: 33280057]

89. Krayem M, Weber Lensing C, Fornander L. Cone-beam computed tomography for primary investigation of wrist trauma provides a new map of fractures of carpal bones. J Hand Surg Eur Vol. 2021;46(6):621–625. doi: 10.1177/17531934211001730. [PubMed: 33757323]

90. Yang T-W, Lin Y-Y, Hsu S-C, et al. Diagnostic performance of cone-beam computed tomography for scaphoid fractures: a systematic review and diagnostic meta-analysis. Sci Rep. 2021;11(1):2587. doi: 10.1038/s41598-021-82351-9. [PubMed: 33510347]

91. Dubreuil T, Mouly J, Ltaief-Boudrigua A, et al. Comparison of Cone-Beam Computed Tomography and Multislice Computed Tomography in the Assessment of Extremity Fractures. J Comput Assist Tomogr. 2019;43(3):372–378. doi: 10.1097/RCT.0000000000000843. [PubMed: 30762657]

92. Hui TCH, Tan GZL, Tan AKW, et al. The use of cone beam CT in achieving unipedicular spinal augmentation. Br J Radiol. 2016;89(1065):20160030. doi: 10.1259/bjr.20160030.

93. Vetter SY, Steffen K, Swartman B, et al. Influence of intraoperative conventional fluoroscopy versus cone beam CT on long-term clinical outcome in isolated displaced talar fractures. J Orthop Surg Res. 2019;14(1):8. doi: 10.1186/s13018-018-1043-3. [PubMed: 30621768]

94. Sebaaly A, Jouffroy P, Emmanuel Moreau P, et al. Intraoperative Cone Beam Tomography and Navigation for Displaced Acetabular Fractures: A Comparative Study. J Orthop Trauma. 2018;32(12):612–616. doi: 10.1097/BOT.0000000000001324. [PubMed: 30299379]

95. Privalov M, Euler F, Keil H, et al. Influence of reduction quality on functional outcome and quality of life in treatment of tibial plafond fractures: a retrospective cohort study. BMC Musculoskelet Disord. 2019;20(1):534. doi: 10.1186/s12891-019-2932-2. [PubMed: 31722696]

96. Reynolds T, Ma YQ, Kanawati AJ, et al. Extended Intraoperative Longitudinal 3-Dimensional Cone Beam Computed Tomography Imaging With a Continuous Multi-Turn Reverse Helical Scan. Invest Radiol. 2022. doi: 10.1097/RLI.0000000000000885.

97. von Arx T, Janner SFM, Hänni S, et al. Radiographic Assessment of Bone Healing Using Cone-beam Computed Tomographic Scans 1 and 5 Years after Apical Surgery. J Endod. 2019;45(11):1307–1313. doi: 10.1016/j.joen.2019.08.008. [PubMed: 31543274]

98. Guggenberger R, Koral E, Zemann W, et al. Cone beam computed tomography for diagnosis of bisphosphonate-related osteonecrosis of the jaw: evaluation of quantitative and qualitative image parameters. Skeletal Radiol. 2014;43(12):1669–1678. doi: 10.1007/s00256-014-1951-1. [PubMed: 24997160]

99. Huber FA, Schumann P, von Spiczak J, et al. Medication-Related Osteonecrosis of the Jaw - Comparison of Bone Imaging Using Ultrashort Echo-Time Magnetic Resonance Imaging and Cone-Beam Computed Tomography. Invest Radiol. 2020;55(3):160–167. 10.1097/RLI.0000000000000617. [PubMed: 31688157]

100. Osgood GM, Thawait GK, Hafezi-Nejad N, et al. Image quality of cone beam computed tomography for evaluation of extremity fractures in the presence of metal hardware: visual grading characteristics analysis. Br J Radiol. 2017;90(1073):20160539. doi: 10.1259/bjr.20160539. [PubMed: 28281784]

101. Johnson TRC. Dual-Energy CT: General Principles. AJR Am J Roentgenol. 2012;199(5_supplement):S3–S8. doi: 10.2214/AJR.12.9116. [PubMed: 23097165]

102. Sherbaf FG, Sair HI, Shakoor D, et al. DECT in Detection of Vertebral Fracture-associated Bone Marrow Edema: A Systematic Review and Meta-Analysis with Emphasis on Technical and Imaging Interpretation Parameters. Radiology. 2021;300(1):110–119. doi: 10.1148/radiol.2021203624. [PubMed: 33876973]

103. Rajiah P, Sundaram M, Subhas N. Dual-Energy CT in Musculoskeletal Imaging: What Is the Role Beyond Gout? AJR Am J Roentgenol. 2019;213(3):493–505. doi: 10.2214/AJR.19.21095. [PubMed: 31039024]

104. Khodarahmi I, Haroun RR, Lee M, et al. Metal Artifact Reduction Computed Tomography of Arthroplasty Implants: Effects of Combined Modeled Iterative Reconstruction and Dual-Energy Virtual Monoenergetic Extrapolation at Higher Photon Energies. Invest Radiol. 2018;53(12):728–735. 10.1097/RLI.0000000000000497. [PubMed: 30015677]
105. Suh CH, Yun SJ, Jin W, et al. Diagnostic performance of dual-energy CT for the detection of bone marrow oedema: a systematic review and meta-analysis. Eur Radiol. 2018;28(10):4182–4194. doi: 10.1007/s00330-018-5411-5. [PubMed: 29679212]
106. Cavallaro M, D'Angelo T, Albrecht MH, et al. Comprehensive comparison of dual-energy computed tomography and magnetic resonance imaging for the assessment of bone marrow edema and fracture lines in acute vertebral fractures. Eur Radiol. 2022;32(1):561–571. doi: 10.1007/s00330-021-08081-8. [PubMed: 34215940]
107. Frellesen C, Azadegan M, Martin SS, et al. Dual-Energy Computed Tomography-Based Display of Bone Marrow Edema in Incidental Vertebral Compression Fractures: Diagnostic Accuracy and Characterization in Oncological Patients Undergoing Routine Staging Computed Tomography. Invest Radiol. 2018;53(7):409–416. doi: 10.1097/RLI.0000000000000458. [PubMed: 29489560]
108. Booz C, Nöske J, Lenga L, et al. Color-coded virtual non-calcium dual-energy CT for the depiction of bone marrow edema in patients with acute knee trauma: a multireader diagnostic accuracy study. Eur Radiol. 2020;30(1):141–150. doi: 10.1007/s00330-019-06304-7. [PubMed: 31350586]
109. Guggenberger R, Gnannt R, Hodler J, et al. Diagnostic performance of dual-energy CT for the detection of traumatic bone marrow lesions in the ankle: Comparison with MR imaging. Radiology. 2012;264(1):164–173. doi: 10.1148/radiol.12112217. [PubMed: 22570505]
110. Palm H-G, Lang P, Hackenbroch C, et al. Dual-energy CT as an innovative method for diagnosing fragility fractures of the pelvic ring: a retrospective comparison with MRI as the gold standard. Arch Orthop Trauma Surg. 2020;140(4):473–480. doi: 10.1007/s00402-019-03283-8. [PubMed: 31612336]
111. Xie C, Ather S, Mansour R, et al. Dual-energy CT in the diagnosis of occult acute scaphoid injury: a direct comparison with MRI. Eur Radiol. 2021;31(6):3610–3615. doi: 10.1007/s00330-020-07604-z. [PubMed: 33341908]
112. Hoover KB, Starks AO, Robila V, et al. Quantitative contrast enhanced dual energy CT to predict avascular necrosis: a feasibility study of proximal humerus fractures. BMC Med Imaging. 2021;21(1):191. doi: 10.1186/s12880-021-00717-x. [PubMed: 34895190]
113. Donders JCE, Wellenberg RHH, Streekstra GJ, et al. Improved diagnostic confidence in evaluating bone non-union using virtual monochromatic dual-energy CT. Eur J Radiol. 2020;132:109159. doi: 10.1016/j.ejrad.2020.109159. [PubMed: 33091864]
114. Fritz J, Henes JC, Fuld MK, et al. Dual-Energy Computed Tomography of the Knee, Ankle, and Foot: Noninvasive Diagnosis of Gout and Quantification of Monosodium Urate in Tendons and Ligaments. In: Semin Musculoskelet Radiol.Vol 20. Thieme Medical Publishers, Inc.; 2016:130–135. doi: 10.1055/s-0036-1579709. [PubMed: 27077593]
115. Shang J, Zhou L-P, Wang H, et al. Diagnostic Performance of Dual-energy CT Versus Ultrasonography in Gout: A Meta-analysis. Acad Radiol. 2022;29(1):56–68. doi: 10.1016/j.acra.2020.08.030. [PubMed: 32980243]
116. Døssing A, Müller FC, Becce F, et al. Dual-Energy Computed Tomography for Detection and Characterization of Monosodium Urate, Calcium Pyrophosphate, and Hydroxyapatite: A Phantom Study on Diagnostic Performance. Invest Radiol. 2021;56(7). doi: 10.1097/RLI.0000000000000756.
117. Tse JJ, Kondro DA, Kuczynski MT, et al. Assessing the Sensitivity of Dual-Energy Computed Tomography 3-Material Decomposition for the Detection of Gout. Invest Radiol. [published online ahead of print, 2022 Apr 22]. doi: 10.1097/RLI.0000000000000879.
118. Gamala M, Jacobs JWG, van Laar JM. The diagnostic performance of dual energy CT for diagnosing gout: a systematic literature review and meta-analysis. Rheumatology (Oxford). 2019;58(12):2117–2121. doi: 10.1093/rheumatology/kez180. [PubMed: 31089688]
119. Baer AN, Kurano T, Thakur UJ, et al. Dual-energy computed tomography has limited sensitivity for non-tophaceous gout: a comparison study with tophaceous gout. BMC Musculoskelet Disord. 2016;17(1):91. doi: 10.1186/s12891-016-0943-9. [PubMed: 26891750]

120. Ahn SJ, Zhang D, Levine BD, et al. Limitations of dual-energy CT in the detection of monosodium urate deposition in dense liquid tophi and calcified tophi. Skeletal Radiol. 2021;50(8):1667–1675. doi: 10.1007/s00256-021-03715-w. [PubMed: 33532938]

121. Guggenberger R. Dual-energy CT in the detection of bone marrow edema in the sacroiliac joints: Is there a case for axial spondyloarthritis? Radiology. 2019;290(1):165–166. doi: 10.1148/radiol.2018182224. [PubMed: 30351250]

122. Kosmala A, Weng AM, Heidemeier A, et al. Multiple Myeloma and Dual-Energy CT: Diagnostic Accuracy of Virtual Noncalcium Technique for Detection of Bone Marrow Infiltration of the Spine and Pelvis. Radiology. 2017;286(1):205–213. doi: 10.1148/radiol.2017170281. [PubMed: 28799843]

123. Kosmala A, Weng AM, Krauss B, et al. Dual-energy CT of the bone marrow in multiple myeloma: diagnostic accuracy for quantitative differentiation of infiltration patterns. Eur Radiol. 2018;28(12):5083–5090. doi: 10.1007/s00330-018-5537-5 [PubMed: 29882069]

124. Thomas C, Schabel C, Krauss B, et al. Dual-Energy CT: Virtual Calcium Subtraction for Assessment of Bone Marrow Involvement of the Spine in Multiple Myeloma. AJR Am J Roentgenol. 2015;204(3):W324–W331. doi: 10.2214/AJR.14.12613. [PubMed: 25714318]

125. Sajja S, Lee Y, Eriksson M, et al. Technical Principles of Dual-Energy Cone Beam Computed Tomography and Clinical Applications for Radiation Therapy. Adv Radiat Oncol. 2020;5(1):1–16. doi: 10.1016/j.adro.2019.07.013. [PubMed: 32051885]

126. Zhao C, Liu SZ, Wang W, et al. Effects of x-ray scatter in quantitative dual-energy imaging using dual-layer flat panel detectors. In: Proc.SPIE.Vol 11595. Published online February 15, 2021. doi: 10.1117/12.2581822

127. Zbijewski W, Sisniega A, Stayman JW, et al. Dual-Energy Imaging of Bone Marrow Edema on a Dedicated Multi-Source Cone-Beam CT System for the Extremities. Proc SPIE Int Soc Opt Eng. 2015;9412. doi: 10.1117/12.2082304.

128. Gang GJ, Zbijewski W, Mahesh M, et al. Image quality and dose for a multisource cone-beam CT extremity scanner. Med Phys. 2018;45(1):144–155. doi: 10.1002/mp.12659 [PubMed: 29121409]

129. Shi L, Lu M, Bennett NR, et al. Characterization and potential applications of a dual-layer flat-panel detector. Med Phys. 2020;47(8):3332–3343. doi: 10.1002/mp.14211. [PubMed: 32347561]

130. Ståhl F, Schäfer D, Omar A, et al. Performance characterization of a prototype dual-layer cone-beam computed tomography system. Med Phys. 2021;48(11):6740–6754. doi: 10.1002/mp.15240. [PubMed: 34622973]

131. Zbijewski W, Gang GJ, Xu J, et al. Dual-energy cone-beam CT with a flat-panel detector: Effect of reconstruction algorithm on material classification. Med Phys. 2014;41(2):21908. doi: 10.1118/1.4863598.

132. Liu SZ, Cao Q, Tivnan M, et al. Model-based dual-energy tomographic image reconstruction of objects containing known metal components. Phys Med Biol. 2020;65(24):245046. doi: 10.1088/1361-6560/abc5a9. [PubMed: 33113519]

133. Bhattarai A, Pouran B, Mäkelä JTA, et al. Dual contrast in computed tomography allows earlier characterization of articular cartilage over single contrast. J Orthop Res. 2020;38(10):2230–2238. doi: 10.1002/jor.24774. [PubMed: 32525582]

134. Kim HJ, Kim JE, Choo J, et al. A clinical pilot study of jawbone mineral density measured by the newly developed dual-energy cone-beam computed tomography method compared to calibrated multislice computed tomography. Imaging Sci Dent. 2019;49(4):295–299. doi: 10.5624/isd.2019.49.4.295. [PubMed: 31915615]

135. Liu S, Zhao C, Herbst M, et al. Feasibility of dual-energy cone-beam CT of bone marrow edema using dual-layer flat panel detectors. In: Proc.SPIE.Vol 12031.Published online February 15, 2021.doi: 10.1117/12.2613211

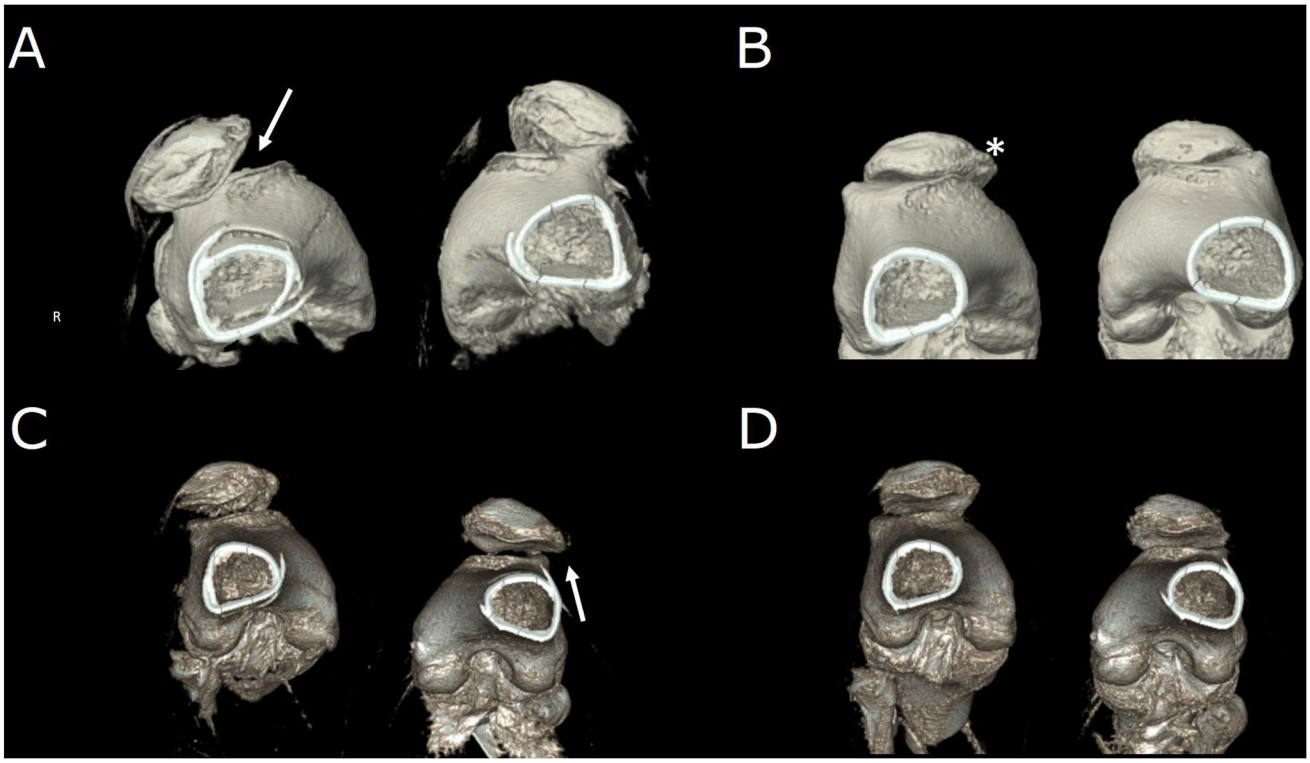

Figure 1.

Pre-and post-operative four-dimensional computed tomography acquisitions of a patient with interval right-sided tibial tubercle osteotomy and medial patellofemoral ligament repair and newly diagnosed left-sided patellar instability. (A) Subluxation in both joints prior to intervention in full extension, worse on the right (arrow). (B) Disappearance of subluxation in full flexion corresponding to the radiographic “J-sign” of maltracking. The presence of osteophyte (*) is consistent with mild-to-moderate secondary osteoarthritis. (C) Full-extension post-operative images show correction of right-sided maltracking with residual left-sided maltracking (arrow). (D) Joints in full flexion post-operatively.

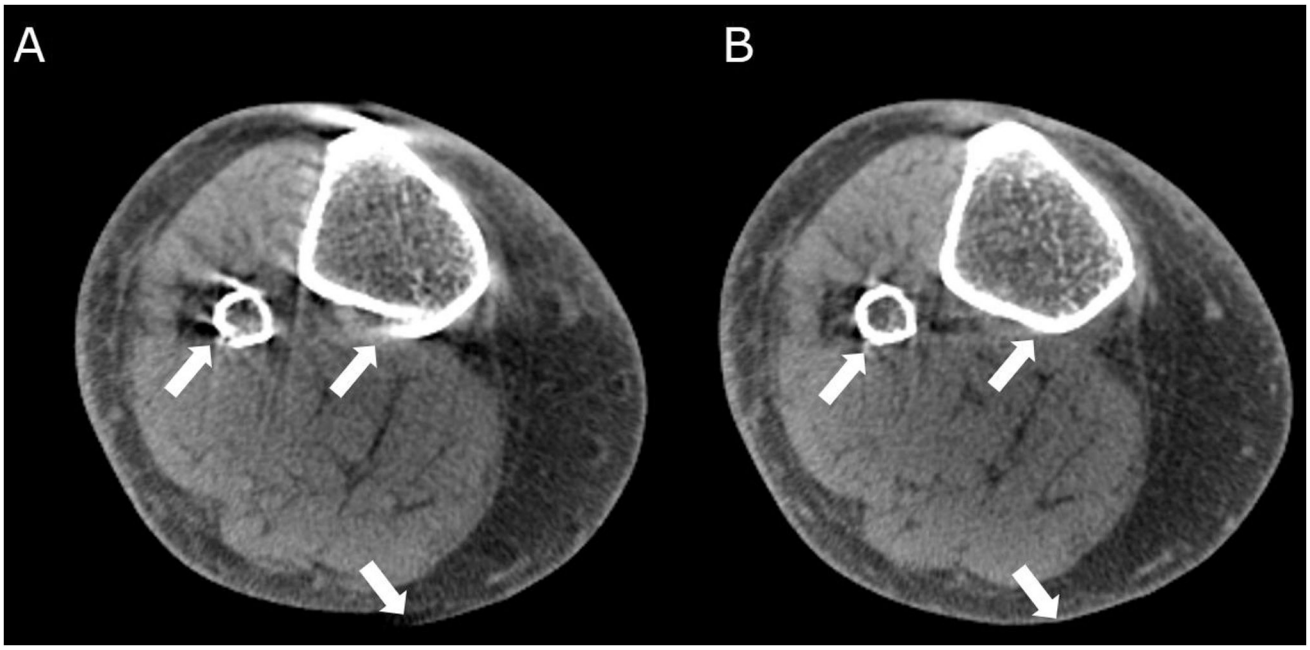

Figure 2.

Autofocus motion compensation in weight-bearing cone-beam computed tomography. (A) Motion-contaminated scan with the characteristic artifact patterns (streaks and doubled contours) (arrows). (B) Autofocus compensation results in substantial artifact reduction (arrows).

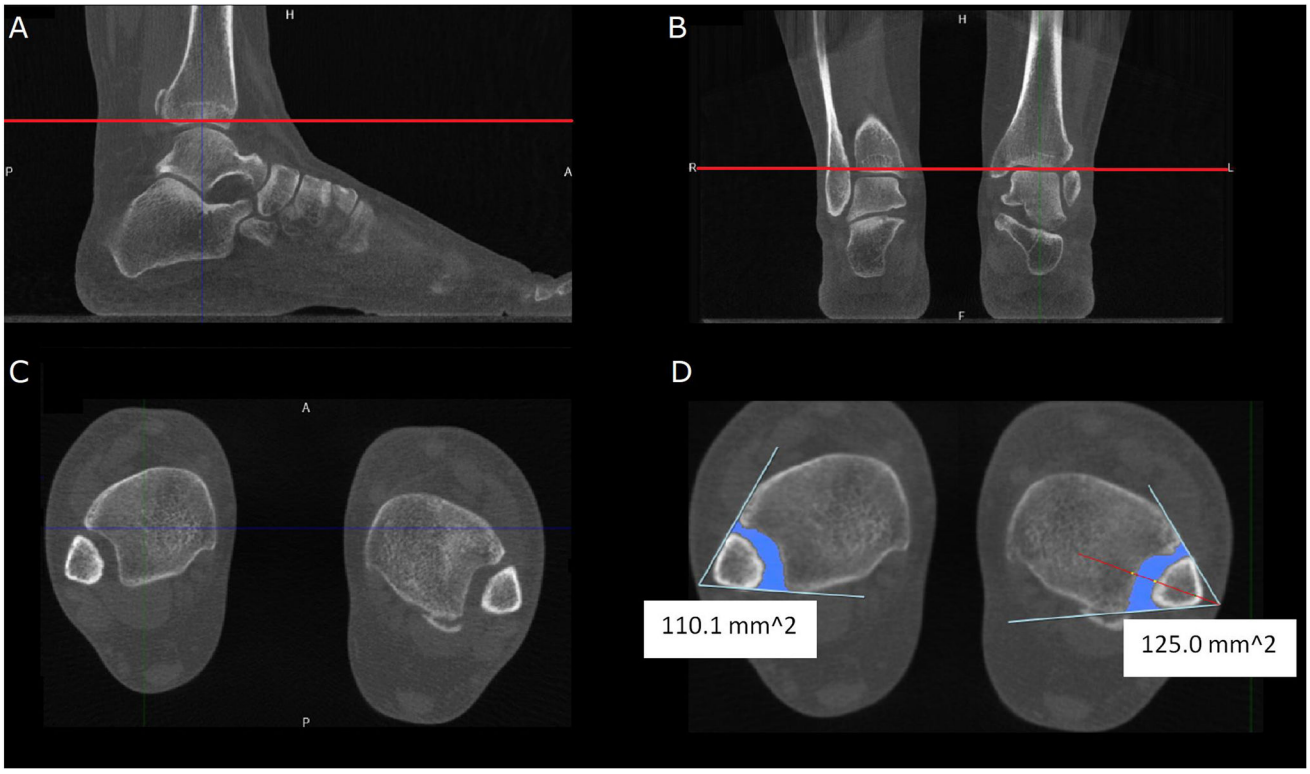

Figure 3.

Weight-bearing cone-beam computed tomography of a 40-year-old presenting with left ankle joint pain and swelling. History revealed two injuries sustained eight years apart, treated conservatively on both occasions. Physical examination revealed neutral heal and foot alignment, but several clinical maneuvers could be provoked. Coronal (A) and sagittal (B) views are used to determine transverse imaging planes above the tibial plafond (red line). (C) and (D) The creation of two intersecting lines, the medial fibular cortex and the lateral tibial incisural cortex helps determine the syndesmotic area on the chosen plane. The left syndesmotic area measures 125mm^{2,} whereas the contralateral side measured 110.1mm^{2} during the weight-bearing examination.

Figure 4:
Three-dimensional rendering of the soft tissue contour of the foot using weight-bearing cone-beam computed tomography of a 56-year-old male suffering from a painful adult acquired flatfoot deformity progressing over eight years. Pain was present around the plantar surface of the heal and sinus tarsi area. Physical exam revealed a flat plantar arch with valgus abduction of the hind-, fore-, and mid-foot regions, tenderness in areas concordant with provided history, limited dorsiflexion, and a hypermobile first ray.

Figure 5.

Measurements from multiplanar reconstructions of weight-bearing cone-beam computed tomography of the patient from figure 4. (A) Measurement of the foot arch angle. (B) First metatarsal base-to-floor angle. (C) ~50% middle facet uncovering, calculated from the division of the measured uncoverage (D2) by the width of the talar middle facet (D1).

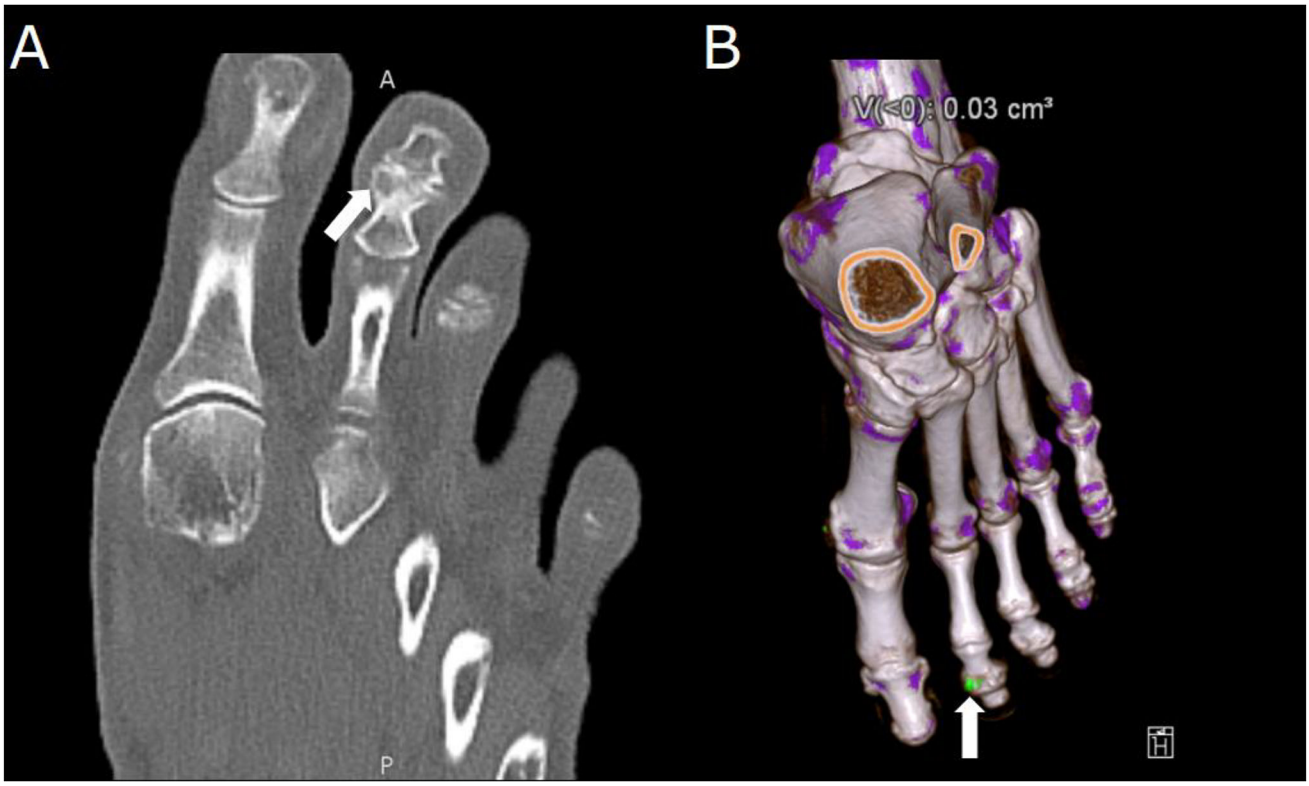

Figure 6.

Dual-energy computed tomography (DECT) of a 65-year-old with polyarticular joint pain and consistently elevated serum uric acid. (A) Demonstration of erosions in the second distal interphalangeal joint characteristic of gout arthropathy (arrow). (B) Material decomposition three-dimensional reconstruction of a DECT acquisition, on which a monosodium urate deposit is seen in green on the same joint (arrow).

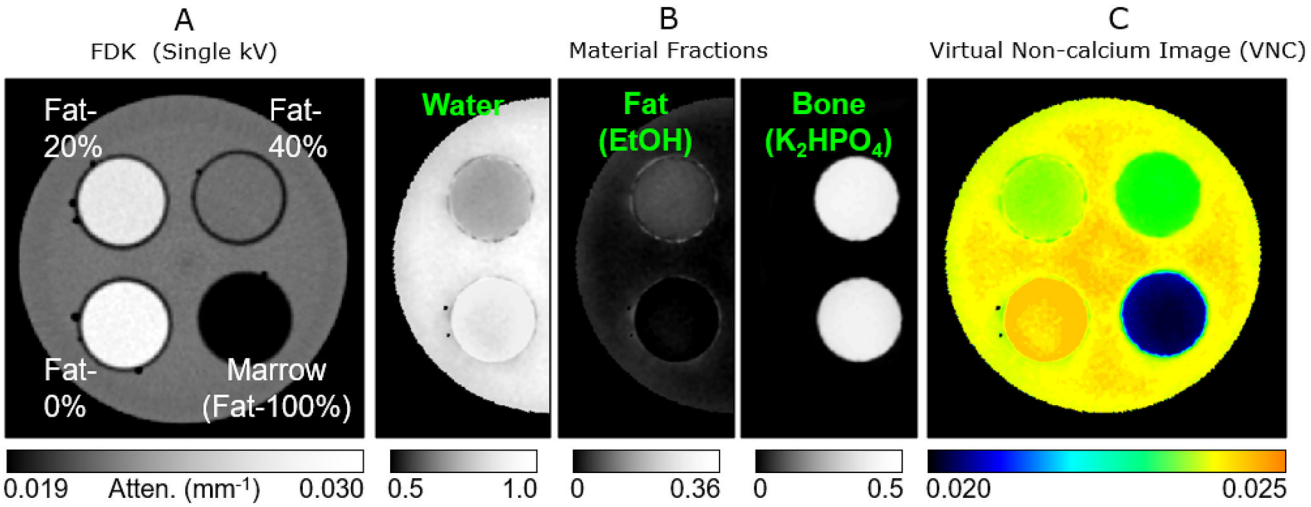

Figure 7.

Experimental feasibility study of bone marrow edema detection using dual-energy cone-beam computed tomography (DE-CBCT). (A) Single-energy image of an experimental phantom containing vials of various mixtures of fat-, water-, and bone-mimicking materials (fat concentration indicated on the image). The concentrations of the three materials cannot be distinguished based on single-energy attenuation. (B) Material concentration maps obtained from a DE-CBCT scan reveal the increased water content (edema-like) in the lower-right insert. (C) Similar to conventional dual-energy computed tomography, DE-CBCT data can be converted into a virtual non-calcium image representing the density of non-mineralized tissues. The images were obtained with 6 cm collimation, and fast Monte Carlo scatter correction.